بسم الله الرحمن الرحيم

Natural Convection From A Vertical Cylinder Of Finite-Height Embedded In A Darcian Fluid-Saturated Porous Medium

الحمل الطبيعى فى وسط مسامى مشبع من اسطوانة رأسية ذات ارتفاع محدود

M. G. WASEL
Mechanical Power Engineering Department, Faculty of Engineering,
Mansoura University, Mansoura, Egypt

خلاصة : فى هذا البحث تمت دراسة الحمل الطبيعى من اسطوانة رأسية محدودة الارتفاع وذلك فى وسط مسامى مشبع بمائع. أفترض أن سطح الاسطوانة محفوظ عند درجة حرارة ثابتة. تم وصف الحمل الطبيعى بواسطة كل من معادلة السريان ومعادلتى دارسى للحركة ومعادلة الطاقة وذلك باستخدام نظام الإحداثيات الأسطوانية. تم وضع هذه المعادلات فى صورة لابعدية وذلك بالتعريف المناسب لكل من المتغيرات المستقلة والتابعة. لطبيعة المعادلات التفاضلية الجزئية الحاكمة للسريان كان لزاما حل هذه المعادلات آنيا على كل حقل السريان. تم حل هذه المعادلات عدديا باستخدام طريقة الفروق المحدودة. تم تصميم برنامج للحاسب الآلى لتنفيذ هذا النموذج النظرى المقترح فى هذه الدراسة. تمت دراسة خواص السريان لاسطوانات ذات ارتفاعات لابعدية بقيم ٢,٥ ، ٥,٠ ، ٧,٥ ، ١٠,٠ وذلك لرقم رايلى ١، ٥ ، ١٠ ، ٢٠ ، ٥٠ . تم حساب كل من رقم نوسلت الموضعى والمتوسط لظروف التشغيل المختلفة. فى هذا البحث تم اقتراح صيغة رياضية لحساب رقم نوسلت المتوسط وذلك كدالة فى كل من طول الاسطوانة ورقم رايلى.

Abstract: In this work, natural convection from a cylinder of finite height is studied. The cylinder is embedded in a fluid-saturated porous medium. Both ends of this cylinder are assumed thermally isolated and the cylindrical surface is maintained at a constant temperature. Steady state condition and isotropic physical properties are assumed. The convective heat transfer process is described by the continuity equation and momentum equations in both axial and radial directions and energy equation. These governing equations are cast in a dimensionless form by the proper definition of the dependent and independent variables. Since the final form of the partial differential governing equations is of an elliptic type, they have to be numerically solved simultaneously through out the flow field. These governing equations are solved, numerically, using the finite difference method. According to this technique, an equivalent set of algebraic linear equations is derived. This set of equations is, in turn, solved using the well-known Gauss-Seidel iterative method. A computer program is designed to solve the present proposed theoretical model. The convective flow properties, in case of cylinder of dimensionless height of 2.5, 5, 7.5 and 10, are studied. Through this study, the Rayleigh number has the values of 1, 5, 10, 20 and 50. Both the local and average Nusselt numbers are calculated for each operating condition. Finally, a correlation is proposed to estimate the average Nusselt number as a function of both cylinder height and Rayleigh number.

1. Introduction

Natural convection heat transfer in a fluid-saturated porous media is of great interest because of its numerous practical applications. Thermal insulation, chemical reactors, underground spread of pollutants and geophysical problems are examples of these applications. Hsieh et al. [1] reported a nonsimilarity solutions for mixed convection from a vertical flat plate embedded in a porous medium. Both surface heating-conditions of variable wall temperature and of variable heat flux were studied. Correlations for local and average Nusselt numbers were presented. Non-Darcian mixed convection along nonisothermal vertical surfaces in porous media was studied by Chien-Hsin et al. [2]. The entire mixed convection regime is covered by a single parameter. A finite difference scheme was used to solve the transformed system of equations. Mixed convection from a vertical cylinder embedded in a porous medium was studied by Aldoss et al. [3]. Nonsimilarity solutions are

Accepted December 12, 1998

obtained for the case of variable wall temperature and variable surface heat flux. The effect of characteristic parameters of the problem on heat transfer is investigated.

Natural convection in a porous medium is a point of interest for many investigators. Non-Darcian natural convection around a horizontal cylinder buried near the surface of a fluid-saturated porous medium was studied by Christopher et al. [4]. The governing equations are solved numerically to obtain the flow field and the temperature distribution around the cylinder. Local and average Nusselt numbers are expressed as a function of cylinder depth, the modified Rayleigh number and Darcy number. Leu and Jin-Yuhjang [5] studied natural convection from a point heat source embedded in a non-Darcian porous medium. Local similarity and modified Keller's Box methods are employed. Natural convection heat transfer between two porous media separated by a vertical wall was studied by Higuera and Pop [6]. The problem of coupled heat transfer by natural convection between two fluid-saturated porous media at different temperatures separated by a vertical conductive wall is investigated analytically and numerically, taking in account the two-dimensional thermal conduction in the separating wall. Higuera [7] studied the conjugate heat transfer across a thin horizontal wall separating two fluid-saturated porous media at different temperatures. Natural convection heat transfer from an isothermal vertical surface to a fluid-saturated thermally stratified porous medium was studied by Angirasa and Pererson [8]. They presented the results of a numerical study of natural convection heat transfer in a stable stratified fluid-saturated low porosity medium. In this investigation, the boundary layer approximations are described and a wide range of ambient thermal stratification levels is considered. Recently, Wasel [9] studied natural convection from a long vertical cylinder embedded in fluid-saturated porous medium. A local similarity solution was obtained. The validity of this solution is restricted to the case of long cylinders.

In the present work, natural convective heat transfer from a constant wall-temperature vertical cylinder of finite-height surrounded by a Darcian fluid-saturated porous medium is investigated. A correlation of the average Nusselt number as a function of both the dimensionless cylinder height and the Rayleigh number is derived.

2. Mathematical Model of the Problem

The mathematical description of the problem and the coordinate system used to investigate the natural convection induced due to a hot finite cylinder embedded in a fluid-saturated porous medium is shown in figure (1). The problem is described by the differential form of the conservation laws of mass, momentum and energy in the cylindrical coordinates. As is shown in the figure, it is reasonable to consider the flow as axisymmetric one. Which means that, the tangential component of velocity and its derivatives vanish in such situation. According to the nature of the examined flow, the derivatives with respect to the angular displacement also vanish. The governing equations of the flow can be, in turn, written as;

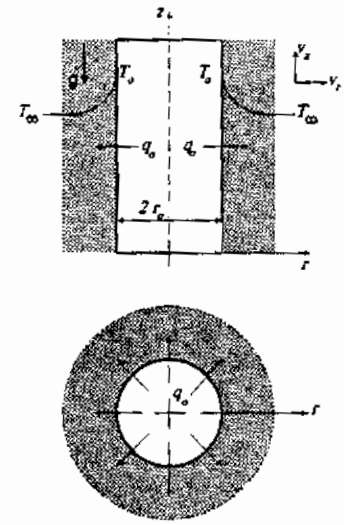

Figure (1) Physical description of the problem

$$\frac{1}{r}\frac{\partial}{\partial r}(r\, v_r)+\frac{\partial v_z}{\partial z}=0 \quad , \tag{1}$$

$$v_r = -\frac{K}{\mu}\frac{\partial p}{\partial r} \quad , \tag{2}$$

$$v_z = -\frac{K}{\mu}\left(\frac{\partial p}{\partial z} + p\, g\right) \quad , \tag{3}$$

$$v_r \frac{\partial T}{\partial r} + v_z \frac{\partial T}{\partial z} = \alpha\left(\frac{\partial^2 T}{\partial r^2} + \frac{1}{r}\frac{\partial T}{\partial r} + \frac{\partial^2 T}{\partial z^2}\right) \tag{4}$$

Where K and μ are the permeability of the porous medium and the dynamic viscosity; respectively. p, ρ, α and g are the pressure, density, thermal diffusivity and gravitational acceleration. Volumetric-averaged radial and axial velocity components and temperature are denoted as v_r , v_z and T; respectively. The physical properties of the medium are assumed to be isotropic and both fluid and solid matrix of the medium are assumed to be in thermal equilibrium [10]. As is shown from equations (2 and 3), the Darcy model is applied to describe the flow in the medium. This model is suitable for a medium of small permeability. To eliminate the pressure, the equations of motion (2 and 3) are differentiated with respect to z and r; respectively, and with some manipulations, they can be reduced to the following single equation;

$$\frac{\partial v_z}{\partial r} - \frac{\partial v_r}{\partial z} = -\frac{K g}{\mu}\frac{\partial \rho}{\partial r} \quad . \tag{5}$$

Moreover, with the aid of the definition of the coefficient of thermal expansion β;

$$\beta = -\left(\frac{1}{\rho}\frac{\partial \rho}{\partial T}\right)_p \quad ,$$

and taking in account the Boussineq approximation, one can eliminate ρ from equation (5) as;

$$\frac{\partial v_z}{\partial r} - \frac{\partial v_r}{\partial z} = \frac{K g \beta}{\upsilon}\frac{\partial T}{\partial r} \quad . \tag{6}$$

Equations (1,4 and 6) are the equations governing the flow, they must satisfy the following boundary conditions;

$$\begin{aligned}
&at \quad r = r_o \ ; \\
&\qquad v_r = v_z = 0 \ and \ T = T_o = constant \quad , \\
&at \quad r \to \infty \ ; \\
&\qquad v_r = 0 \ and \ T = T_\infty = ambient\ temp. \quad , \\
&at \quad r \neq r_o \ and \ z = 0 \ ; \\
&\qquad v_z = 0 \ and \ T = T_\infty \quad ,
\end{aligned} \tag{7}$$

$$at \quad r \neq r_o \ and \ z = l \ ;$$

$$v_z = 0 \ and \ T = T_\infty \ .$$

Where r_o and l are the cylinder radius and height; respectively. T_o and T_∞ are the temperature at the cylinder wall and that far from the wall. In the forgoing boundary conditions, the heat is assumed to be transferred from the cylindrical surface area only and the temperature of the surface is maintained constant. Moreover, heat transfer in the axial direction is neglected. This assumption is, reasonably, valid in case of relatively long cylinder or in case of insulated base and top of cylinder. One defines the stream function ψ such that it satisfies the continuity equation (1). Accordingly ψ is defined as;

$$v_r = -\frac{1}{r}\frac{\partial \psi}{\partial z} \qquad \text{and} \qquad v_z = \frac{1}{r}\frac{\partial \psi}{\partial r} \ . \tag{8}$$

Substitution of equations (8) into equations (4 and 6) leads to;

$$\frac{1}{r}\frac{\partial^2 \psi}{\partial r^2} - \frac{1}{r^2}\frac{\partial \psi}{\partial r} + \frac{1}{r}\frac{\partial^2 \psi}{\partial z^2} = \frac{K g \beta}{\upsilon}\frac{\partial T}{\partial r} \ , \tag{9}$$

$$-\frac{1}{r}\frac{\partial \psi}{\partial z}\frac{\partial T}{\partial r} + \frac{1}{r}\frac{\partial \psi}{\partial r}\frac{\partial T}{\partial z} = \alpha\left(\frac{\partial^2 T}{\partial r^2} + \frac{1}{r}\frac{\partial T}{\partial r} + \frac{\partial^2 T}{\partial z^2}\right) \ . \tag{10}$$

With the aid of equations (7 and 8), one can derive the boundary conditions, which must be satisfied by equations (9 and 10). These boundary conditions take the form;

$$at \quad r = r_o \ ;$$

$$\psi = 0 \ and \ T = T_o = constant \ ,$$

$$at \quad r \to \infty \ ;$$

$$\frac{\partial \psi}{\partial z} = 0 \ and \ T = T_\infty = ambient \ temp. \ , \tag{11}$$

$$at \quad r \neq r_o \ and \ z = 0 \ ;$$

$$\frac{\partial \psi}{\partial r} = 0 \ and \ T = T_\infty \ ,$$

$$at \quad r \neq r_o \ and \ z = l \ ;$$

$$\frac{\partial \psi}{\partial r} = 0 \ and \ T = T_\infty$$

In order to put equations (9 and 10) and their boundary conditions (11) in a dimensionless form, one can introduce the following definitions of the dimensionless dependent and independent variables as;

$$R = \frac{r}{r_o} ; Z = \frac{z}{r_o} ; f = \frac{\psi}{\alpha r_o} \text{ and } \theta = \frac{T - T_\infty}{T_o - T_\infty} \quad . \tag{12}$$

Accordingly, the dimensionless form of the momentum and energy equations and their boundary conditions can be written as;

$$\frac{1}{R}\frac{\partial^2 f}{\partial R^2} - \frac{1}{R^2}\frac{\partial f}{\partial R} + \frac{1}{R}\frac{\partial^2 f}{\partial Z^2} = Ra \frac{\partial \theta}{\partial R} \quad , \tag{13}$$

$$-\frac{1}{R}\frac{\partial f}{\partial Z}\frac{\partial \theta}{\partial R} + \frac{1}{R}\frac{\partial f}{\partial R}\frac{\partial \theta}{\partial Z} = \frac{\partial^2 \theta}{\partial R^2} + \frac{1}{R}\frac{\partial \theta}{\partial R} + \frac{\partial^2 \theta}{\partial Z^2} \quad . \tag{14}$$

With the boundary conditions;

at $R = 1$;

$$f = 0 \text{ and } \theta = 1 \quad .$$

at $R \to \infty$;

$$\frac{\partial f}{\partial Z} = 0 \text{ and } \theta = 0 \quad ,$$

at $R \neq 1$ *and* $Z = 0$; (15)

$$\frac{\partial f}{\partial R} = 0 \text{ and } \theta = 0 \quad ,$$

at $R \neq 1$ *and* $Z = L$;

$$\frac{\partial f}{\partial R} = 0 \text{ and } \theta = 0 \quad .$$

Where f and θ are the dimensionless stream function and dimensionless temperature; respectively. L is the dimensionless cylinder height and is defined as l / r_o. Z and R are dimensionless axial- and radial- direction coordinates and Ra is Rayleigh number, which is defined as;

$$Ra = \frac{K g \beta (T_o - T_\infty) r_o}{\alpha \upsilon}$$

By solving equations (13 and 14), the values of the dimensionless stream function and dimensionless temperature can be determined through out the flow field. Accordingly, the dimensionless axial and radial components of velocity can be determined, using equations (8 and 12), as follows;

$$V_r = \frac{v_r}{\alpha / r_o} = -\frac{1}{R}\frac{\partial f}{\partial Z} \quad \text{and} \quad V_z = \frac{v_z}{\alpha / r_o} = \frac{1}{R}\frac{\partial f}{\partial R} \tag{16}$$

Where V_r and V_z are the dimensionless radial- and axial-components of velocity. Moreover, one can calculate the local Nusselt number according to the following expression as;

$$Nu = -\left(\frac{\partial \theta}{\partial R} \right)_{R=1} \quad , \tag{17}$$

where Nu is local Nusselt number based on the cylinder radius r_o, which is defined as ;

$$Nu = \frac{h\, r_o}{k} \quad ,$$

and k is thermal conductivity of the medium and h is the local heat transfer coefficient, which is defined as;

$$h = \frac{q_o}{(T_o - T_\infty)} \quad \text{and} \quad q_o = -k \left(\frac{\partial T}{\partial r} \right)_{r=r_o} \quad .$$

Where q_o is heat flux at the cylinder wall.

3. Numerical Procedure

The governing equations (13 and 14) are solved numerically using the finite difference technique. According to this technique, the partial differential equations describing the flow are transformed to associated sets of linear algebraic equations. To carry out this approximation, the derivatives involved in the governing equations are approximated by finite divided differences, where the considered flow field is covered by variable-step size grid. This network is shown in figure (2). This grid consists of two groups of lines; the first group is parallel to the cylinder axis and the other one is normal to it. The identifier of axis-parallel lines is denoted by k, where k takes the values from 1 to n. n is the total number of columns. The identifier of the normal lines is denoted by j, where j changes from 1 to the total number of rows (m). Any node on the network is identified by the identifier i, where i is defined as a function of j and k according to the relation;

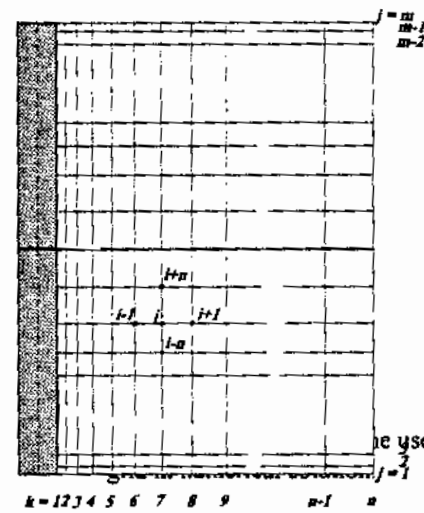

$$i = n\ (j - 1) + k \tag{18}$$

As in the figure, the step size in both directions is taken changeable such that the step size near the wall (in R-direction) and at both ends of the cylinder (in Z-direction) are smaller. The step size $(\Delta R)_i$ and $(\Delta Z)_i$ are calculated according to the following relations;

$$(\Delta R)_{i+1} = \gamma_r\ (\Delta R)_i \quad ,$$

for the lower half of the cylinder; $(\Delta Z)_{i+n} = \gamma_z \, (\Delta Z)_i$,

for the upper half of the cylinder; $(\Delta Z)_{i+n} = (\Delta Z)_i / \gamma_z$.

Where both γ_r and γ_z takes values greater than unity

Considering a general interior point i as shown in figure (3), one can approximate for the variable f the first and second derivatives with respect to R as;

$$\left(\frac{\partial f}{\partial R}\right)_i = \frac{f_{i+1} + (\gamma_r - 1)\, f_i - \gamma_r\, f_{i-1}}{2\, \gamma_r\, (\Delta R)} \quad ,$$

$$\left(\frac{\partial^2 f}{\partial R^2}\right)_i = \frac{f_{i+1} - (1+\gamma_r)\, f_i + \gamma_r\, f_{i-1}}{\gamma_r^2\, (\Delta R)^2} \quad ,$$

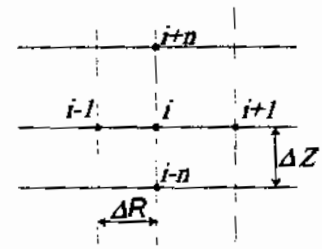

Figure (3) A part of grid showing a general node i and its neighbor nodes .

In the same manner, one can derive the rest of the derivatives. As it is clear, the foregoing derivatives are similar to the formulas of central finite differences if $\gamma_r = 1$ [11]. Substitution in final form of governing equations (13 and 14); leads to the following two equivalent sets of difference equations;

$$A_i\, f_{i+1} + B_i\, f_i + C_i\, f_{i-1} + D_i\, f_{i+n} + E_i\, f_{i-n} + F_i = 0 \quad , \qquad (19)$$

$$A_i^*\, \theta_{i+1} + B_i^*\, \theta_i + C_i^*\, \theta_{i-1} + D_i^*\, \theta_{i+n} + E_i^*\, \theta_{i-n} = 0 \quad . \qquad (20)$$

Equation (19) is the equivalent difference equation of the momentum equation (13), while equation (20) is associated with the energy equation (14). These two recursive relations are valid for all interior nodes of the grid. The coefficients of these equations are defined through the following relations;

$$A_i = \gamma_z^2\, (\Delta Z)^2 \cdot [R_i - 0.5\, \gamma_r\, (\Delta R)]$$

$$B_i = -R_i\, \gamma_z^2\, (1+\gamma_r)\, (\Delta Z)^2 - 0.5\, \gamma_r\, \gamma_z^2\, (\gamma_r - 1)\, (\Delta R)\, (\Delta Z)^2 - R_i\, \gamma_r^2\, (\gamma_z + 1)\, (\Delta R)^2$$

$$C_i = R_i\, \gamma_r\, \gamma_z^2\, (\Delta Z)^2 + 0.5\, \gamma_r^2\, \gamma_z^2 (\Delta R)\, (\Delta Z)^2$$

$$D_i = R_i\, \gamma_r^2\, (\Delta R)^2$$

$$E_i = R_i\, \gamma_r^2\, \gamma_z\, (\Delta R)^2$$

$$F_i = -0.5\, \gamma_r\, \gamma_z^2\, (\Delta R)\, (\Delta Z)^2\, R_i^2\, Ra \cdot [\theta_{i+1} + (\gamma_r - 1)\, \theta_i - \gamma_r\, \theta_{i-1}]$$

$$A^*_i = -0.25\,\gamma_r\,\gamma_z\,(\Delta R)\,(\Delta Z)\,[f_{i+n} + (\gamma_z - 1)\,f_i - \gamma_z\,f_{i-n}] - \gamma_z^2\,(\Delta Z)^2\,R_i - 0.5\,\gamma_r\,\gamma_z^2\,(\Delta R)\,(\Delta Z)^2$$

$$B^*_i = -0.25\,(\gamma_r - 1)\,\gamma_r\,\gamma_z\,(\Delta R)\,(\Delta Z)\,[f_{i+n} + (\gamma_z - 1)\,f_i - \gamma_z\,f_{i-n}] + 0.25\,\gamma_r\,\gamma_z\,(\gamma_r - 1)\,(\Delta R)\,(\Delta Z)\,[f_{i+1} + (\gamma_r - 1)\,f_i - \gamma_r\,f_{i-1}] + \gamma_z^2\,(\gamma_r + 1)\,(\Delta Z)^2\,R - 0.5\,\gamma_z^2\,\gamma_r\,(\gamma_r - 1)\,(\Delta R)\,(\Delta Z)^2 + \gamma_r^2\,(\gamma_z + 1)\,R\,(\Delta R)^2$$

$$C^*_i = 0.25\,\gamma_r^2\,\gamma_z\,(\Delta R)\,(\Delta Z)[f_{i+n} + (\gamma_z - 1)\,f_i - \gamma_z\,f_{i-n}] - \gamma_r\,\gamma_z^2\,R\,(\Delta Z)^2 + 0.5\,\gamma_r^2\,\gamma_z^2\,(\Delta R)\,(\Delta Z)^2$$

$$D^*_i = 0.25\,\gamma_r\,\gamma_z\,(\Delta R)(\Delta Z)[f_{i+1} + (\gamma_r - 1)\,f_i - \gamma_r\,f_{i-1}] - \gamma_r^2\,R\,(\Delta R)^2$$

$$E^*_i = -0.25\,\gamma_r\,\gamma_z^2\,(\Delta R)(\Delta Z)[f_{i+1} + (\gamma_r - 1)\,f_i - \gamma_r\,f_{i-1}] - \gamma_r^2\,\gamma_z\,R\,(\Delta R)^2$$

According to equations (15) and referring to figure (2), the values of the variables f and θ at the nodes which lie at the mesh boundaries are as follows;

for $k = 1$ (corresponding to $R = 1$);

$$f = 0 \quad \text{and} \quad \theta = 1 \quad ,$$

for $k = n$ (corresponding to $R \to \infty$);

$$f_i = f_{i+n} \quad \text{and} \quad \theta = 0 \quad , \qquad (21)$$

for $j = 1$ and $k \neq 1$ (corresponding to $R \neq 1$ *and* $Z = 0$);

$$f_i = f_{i+1} \quad \text{and} \quad \theta = 0 \quad ,$$

for $j = m$ and $k \neq 1$ (corresponding to $R \neq 1$ *and* $Z = L$);

$$f_i = f_{i-1} \quad \text{and} \quad \theta = 0 \quad .$$

The two sets of equations (19 and 20) are solved simultaneously using the well-known iterative method by Gauss-Seidel. Seeking for linearity of equations (19 and 20), the coefficients of both sets are taken constant throughout each iteration process. Accordingly, these coefficients are evaluated based on the associated values of variables obtained by the previous iteration. According to the definitions of dimensionless radial and axial component of velocity and local Nusselt number [equations (16 and 17)] and referring to figures (3 and 4), one can determine their values numerically as;

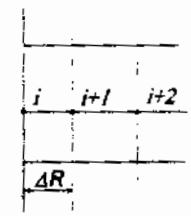

Figure (4) Notations used for calculation of Nusselt number.

$$V_i = \frac{1}{R_i}\,\frac{f_{i+1} + (\gamma_r - 1)\,f_i - \gamma_r\,f_{i-1}}{2\,\gamma_r\,(\Delta R)} \quad ,$$

$$V_r = -\frac{1}{R_i}\,\frac{f_{i+n} + (\gamma_z - 1)\, f_i - \gamma_z\, f_{i-n}}{2\,\gamma_z\,(\Delta Z)} \qquad (22)$$

$$Nu = -\frac{-\theta_{i+2} + 4\,\theta_{i+1} - 3\,\theta_i}{(\gamma_r + 1)\,(\Delta R)}$$

4. Results and Discussions

A computer program is designed according to the previously explained technique. The proper numerical value of the maximum radial distance associated with $R \to \infty$ is found to be 15. Through out all the carried out computer runs, the average step size in both directions (ΔR and ΔZ) is taken as 0.2, while the ratio between the size of two successive steps (γ_r and γ_z) is taken as 1.1. The mesh size is taken as 13x75, 25x75, 37x75 and 51x75 for the cylinders of dimensionless height of 2.5, 5, 7.5, 10; respectively.

The dimensionless stream function contours and isotherms are shown in figure (5); for a dimensionless cylinder height of 10 and Rayleigh number of 10. Referring to [figure (5-a)], the values of the stream function change rapidly near the cylinder wall, especially around the middle of the cylinder. Also near the cylinder wall the contour lines are almost parallel to the cylinder axis. As it is expected, these lines are nearly parallel to the R-axis near both ends of cylinder. Considering the temperature-contours figure (5-b), the temperature gradient near the lower end of the cylinder has very high value. Far from the cylinder wall, the value of gradient decreases in upward direction till it reaches minimum value at a value of Z of about 8. For a radial distance R higher than 9, there is no effect of the hot wall of cylinder (no buoyancy force) and there the gravitational force is dominant.

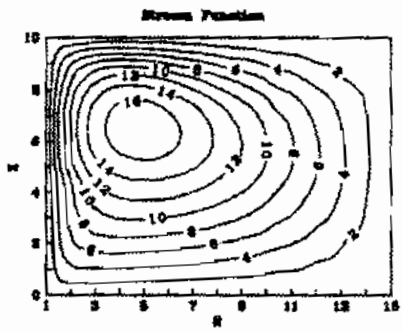

Figure (5-a)

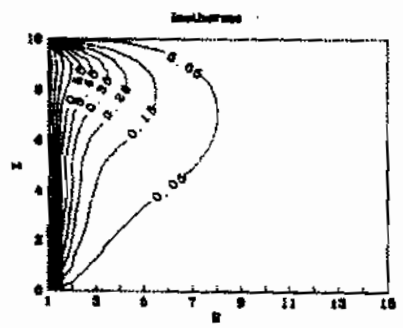

Figure (5-b)

Figure (5) Dimensionless stream function-lines and isotherms for Rayleigh number of 10 and dimensionless cylinder height of 10.

Figure (6) shows the dimensionless velocity distribution in both the radial and axial directions. Considering the radial component of the velocity figure (6-a), this velocity in the lower half of flow field is negative (toward the cylinder). In the upper half, the radial velocity is positive. As it is clear, the flow field is divided into two zones at $Z \approx 6$. Considering figure (6-b), the dimensionless axial component is positive in the left part of the flow field (adjacent to the cylinder), while in the right part it is negative (in downward direction).

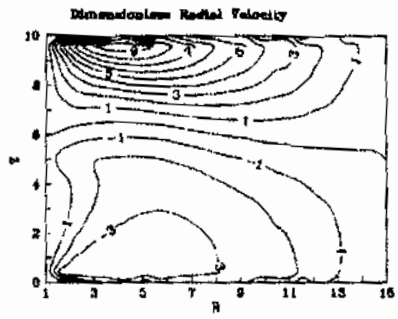

Figure (6-a)

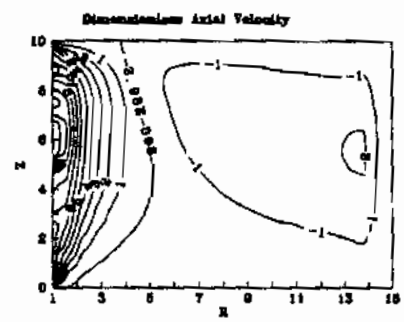

Figure (6-b)

Figure (6) Contours of the dimensionless radial and axial components of the velocity.

Figure (7) shows the dimensionless temperature distribution at three different axial positions. The first one is taken near the bottom of the cylinder (Z=0.543), the second one is at the middle of the cylinder (Z=2.5) and the third curve is taken near the top end of the cylinder (Z=4 457). In general, the temperature decreases continuously and rapidly near the cylinder wall (R≈3 0), then slowly till it takes an asymptotic value of zero at dimensionless radial distance of about nine.

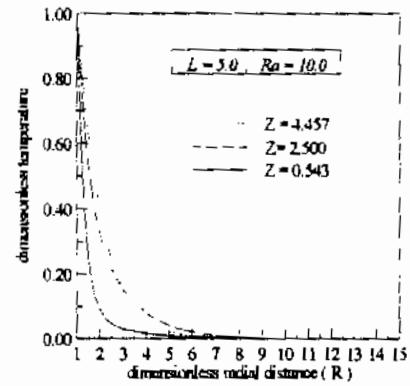

Figure (7) Dimensionless temperature at different axial positions

Figure (8) shows the dimensionless radial and axial components of velocity at the same three axial positions. Considering the dimensionless radial velocity; figure (8-a), near the bottom, the velocity adjacent to the cylinder decreases rapidly till it reaches a minimum value then it increases relatively slowly until it reaches a value of zero. At the middle of the cylinder, the behavior of velocity is similar to that near the bottom of cylinder Near the top, radial velocity increases rapidly till it reaches a maximum value at R≈3.0 then it decreases gradually till it reaches a value of zero. Considering the dimensionless axial velocity [figure (8-b)] and for all axial positions, the velocity in the zone adjacent to the cylinder is positive (in upward direction). Then it decreases rapidly to a negative value. This value is smaller for lower values of the axial position Finally, the axial velocity takes an asymptotic value of zero.

Four cylinders of dimensionless heights of 2.5, 5, 7.5 and 10 are examined in this work. In figure (9), the local Nusselt number for the cylinder of dimensionless height of 7 5 is presented. The Nusselt number goes to infinity at both ends of the cylinder for all values of Rayleigh number, and then it decreases rapidly to smaller values. The value of Nusselt number at the lower half of cylinder is greater than that at the upper half. The average Nusselt number for each cylinder for different values of Rayleigh number is calculated according to the following definition;

$$\overline{Nu} = \frac{1}{L}\int_0^L Nu\, dZ \quad .$$

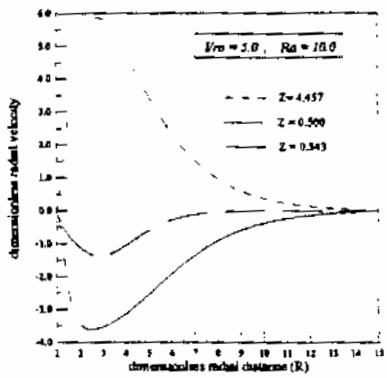

Figure (8-a)

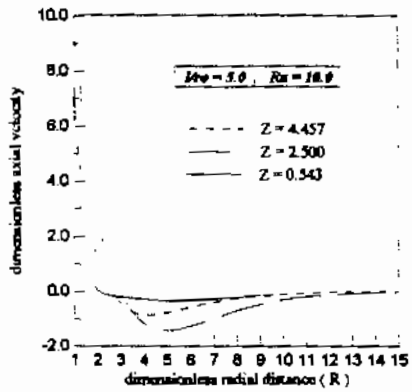

Figure (8-b)

Figure (8) Dimensionless radial and axial velocity at different axial positions

A correlation of the average Nusselt number as function of both the Rayleigh number and the dimensionless cylinder height was derived as;

$$\overline{Nu} = 380\ (Ra)^{0.011}\ (L)^{-1.67} \qquad (23)$$

Figure (10) shows a comparison between the calculated average Nusselt number and that calculated from the foregoing correlation, equation (23). This correlation fits the calculated data better for higher values of dimensionless cylinder length (L). The effect of Rayleigh number is very small compared with the effect of cylinder length, perhaps because of the bigher weight of local Nusselt number at cylinder ends relative to that along the rest of the cylinder height [see figure (9)].

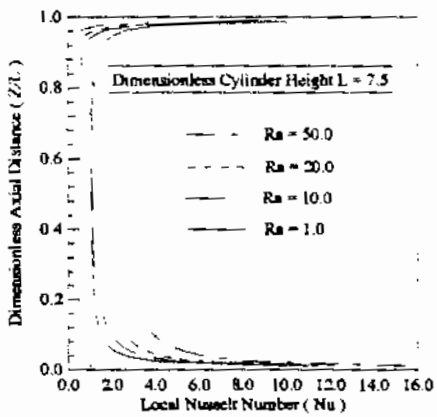

Figure (9) Local Nusselt number at different values of Rayleigh number

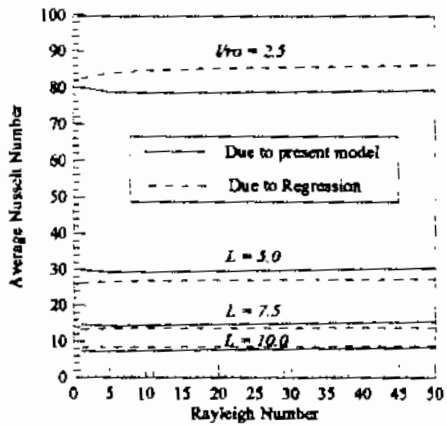

Figure (10) Calculated average Nusselt number and that due to the correlation

Figure (11) shows a comparison between the present results and those of [8]. Since the results of [8] are obtained for an isothermal vertical surface, a qualitative comparison is only possible. Figure (11-a) shows the dimensionless axial velocity obtained in the present

work and that after [8]. The dimensionless axial velocity in the present work is defined according to equation (16) as; $V_z = v_z \cdot r_o / \alpha$, while in reference [8] it is defined as; $Vz = v/V_c$. Where V_c is a convective velocity given by; $V_c = g\ \beta\ (T_o - T_\infty)\ K/\upsilon$. As it is clear, both curves of the present work and of [8] have the same behavior, near the surface they have their maximum value and then their value decreases rapidly, thereafter the velocity decreases slowly till it reaches an asymptotic value of about zero far from the surface. Figure (11-b) shows the dimensionless temperature versus the distance normal to the surface (it is radial in the present work). Both the dimensionless temperatures obtained in the present work and that due to [8] have the same trend.

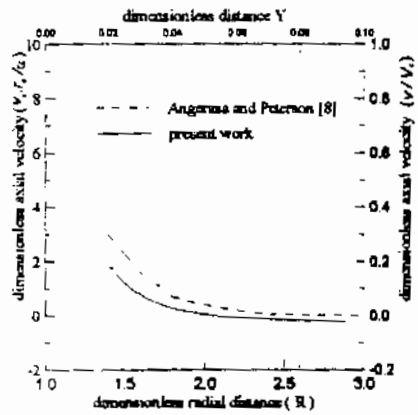

Figure (11-a)

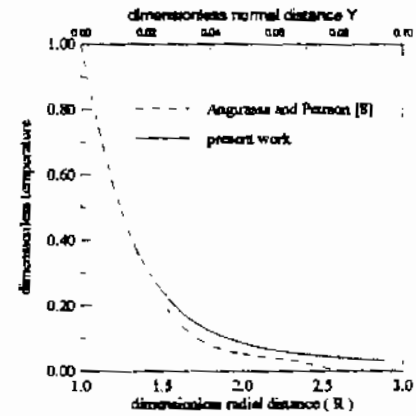

Figure (11-b)

Figure (11) Comparison between present results and those of reference [8]

Although the study of Wasel [9] is for the free convective heat transfer from a long cylinder, a comparison between the present work and that of [9] is presented in figure (12). It is clear from figure (12-a) that, the values of Nusselt number in the case of the long cylinder (L=10) are closer to those of [9]. Because of the long cylinder assumption made in [9], the simplification of the governing equations by neglecting some terms of the original form of those equations is, reasonably, possible. According to this simplification, a local similarity solution for long cylinders is achieved. As it is clear in figure (12-b), this solution is not valid in case of cylinders of finite height, especially in case of higher values of Rayleigh number.

5. Conclusions

In this work, a theoretical model ia proposed to analyze the natural convection in a porous medium. The effects of both Rayleigh number and cylinder height are studied. A correlation of average Nusselt number as a function of the cylinder height and Rayleigh number is derived. In this model, no heat is transferred from both ends of the cylinder. Accordingly, this model is more suitable for the case of relatively long cylinders as well as for the cylinders of insulated base and top.

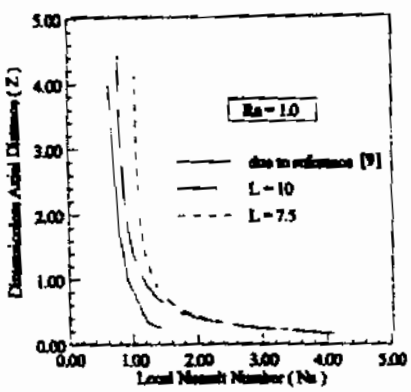

Figure (12-a)

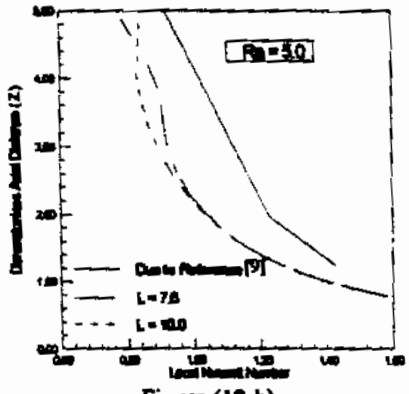

Figure (12-b)

Figure (12) Comparison between the present results and those after reference [9]

Nomenclature

f	dimensionless stream function, $f = \psi \ / \ (\alpha \ z)$
h	heat transfer coefficient, $h = q_o \ / \ (T_o - T_\infty)$
g	gravitational acceleration
K	permeability of porous medium
k	thermal conductivity of fluid-saturated porous medium, $k = \phi \ k_f + (1-\phi) k_s$
k_f	thermal conductivity of fluid constituent
k_s	thermal conductivity of solid constituent
L	dimensionless cylinder height, $L = l/r_o$
l	cylinder height
Nu	local Nusselt number
$\overline{Nu}$	average Nusselt number
p	pressure
q_o	heat flux at cylinder wall
R, Z	dimensionless radial and axial coordinates
Ra	Rayleigh number based on cylinder radius, $Ra = K \ g \ \beta \ (T_o - T_\infty) \ r_o / \alpha \ \nu$
r, z	radial and axial coordinates
r_o	cylinder radius
T	temperature of fluid-saturated porous medium
T_o	temperature of cylinder surface
T_∞	temperature of porous medium far from the surface
V_r, V_z	dimensionless radial and axial components of velocity
v_r, v_z	radial and axial components of velocity

Greek symbols

α	thermal diffusivity of homogenous porous medium, $\alpha = k \ / \rho_f \ c_{p_f}$

β coefficient of thermal expansion, $\beta = -\left(\frac{1}{\rho}\frac{\partial \rho}{\partial T}\right)_p$

ϕ porosity of porous medium, ϕ = *pores volume / total volume*

μ, ν dynamic and kinematic viscosity

θ dimensionless temperature, $(T - T_\infty)/(T_o - T_\infty)$

ψ Stream function

References

1. J. C. Hsieh, T. S. Chen and B. F. Armaly, Nonsimilarity solutions for mixed convection from vertical surfaces in porous media: variable surface temperature or heat flux, Int. J. Heat Mass Transfer, Vol. 36, No. 6, pp. 1485-1493, 1993.
2. Chien-Hsin Chen, T. S. Chen and Cha'o-Kuang Chen, Non-Darcy mixed convection along nonisothermal vertical surfaces in porous media, Int. J. Heat Mass Transfer, Vol. 39, No. 6, pp. 1157-1164, 1996.
3. T. K. Aldoss, M. A. Jarrah and B. J. Al-Sha'er, Mixed convection from a vertical cylinder embedded in a porous medium: non-Darcy model, Int. J. Heat Mass Transfer, Vol. 39,No. 6, pp. 1141-1148,1996.
4. D. M. Christopher and B. -X. Wang, Non-Darcy natural convection around a horizontal cylinder buried near the surface of a fluid-saturated porous medium, Int. J. Heat Mass Transfer, Vol. 36, No. 15, PP 3663-3669, 1993.
5. Jin-Sheng Leu and Jiin-Yuhjang, The natural convection from a point heat source embedded in a non-Darcian porous medium, Int. J. Heat Mass Transfer, Vol. 38, No. 6, pp. 1097-1104, 1995.
6. F. J. Higuera and I. Pop, Conjugate natural convection heat transfer between two porous media separated by a vertical wall, Int., J., Heat Mass Transfer, Vol. 40, No.1, pp. 123-129, 1997.
7. F. J. Higuera, Conjugate natural convection heat transfer between two porous media separated by a horizontal wall, Int. J. Heat Mass Transfer, Vol. 40, No. 13, pp. 3157-3161,1997.
8. D. Angirasa and G. P. Peterson, Natural convection heat transfer from an isothermal vertical surface to a fluid saturated thermally stratified porous medium, Int. J. Heat Mass Transfer, Vol. 40, No. 18, pp. 4329-4335, 1997.
9. M. G. Wasel, Local similarity solution of the free convection from a long vertical cylinder embedded in a darcian fluid-saturated porous medium, Mansoura Engineering Journal (MEJ), Vol. 23, No. 2, pp. M16-M25, June 1998.
10. Adrian Bejan, Convection Heat Transfer, A WILEY-INTERSCIENCE PUBLICATION, JOHN WILEY & SONS, 1984.
11. S. C. Chapra, R. P. Canale, Numerical methods for engineers, McGraw-Hill Book Company, 1987.